

# Error budget of terrestrial laser scanning: influence of the incidence angle on the scan quality

Sylvie Soudarissanane, Jane van Ree,  
Alexander Bucksch and Roderik Lindenbergh.

Delft Institute of Earth Observation and Space Systems (DEOS), Delft University of Technology,  
Kluyverweg 1, 2629 HS Delft, The Netherlands  
S.S.Soudarissanane@tudelft.nl

## Abstract

High spatial resolution and fast capturing possibilities make 3D terrestrial laser scanners widely used in engineering applications and cultural heritage recording. Phase based laser scanners can measure distances to object surfaces with a precision in the order of a few millimeters at ranges between 1 and 80 m. However, the object surface orientation influences the quality of single points in the point cloud data. This paper investigates the performances of a FARO LS880-HE80 laser scanner in measuring a surface oriented at several angular positions under stable conditions. For this purpose one medium-density fibre board and one white coated plywood board are scanned from different angles. By reconstructing the incidence angle of the laser beam corresponding to each individual scan point, an in practice continuous range of angles is obtained from only a limited number of scans. This allows us to study the noise level and relative intensity as a function of the scan angle. In general, the obtained results match the results as may be expected from scattering theory, but it is also shown that saturation has high impact for especially near perpendicular incidence angles. Modeling the incidence angle induced error component seems a feasible step in the construction of the total error budget of individual scan points.

## 1 Introduction

The terrestrial laser scanner surveying technology is increasingly being used for representing and analyzing 3D objects in a wide range of engineering applications. One of the main applications of the terrestrial laser scanner is the visualization, modeling and monitoring of man made structures like buildings. Especially surveying applications require on one hand a quickly obtainable, high resolution point cloud but also need observations with a known and well described quality. The phase based measurement technique, where the phase of a multi-modulated wave determines the distance to an object, is used in recent years mainly because of its high speed. Meanwhile, a complete quality description of individual scan points is still under active research.

A laser scan provides a spherical representation of the surroundings with the center of the terrestrial laser scanner as the origin of the coordinate system. It uses the reflection of the laser beam on the object surface to acquire a range measurement as well as the intensity value of the reflected light. The accuracy of the range measurement is dependant on the scanner mechanism precision, but also on the properties of the scanned surface (e.g. roughness, reflectivity, color, angle) and the conditions of the experiment environment (e.g. ambient light, humidity, temperature, atmosphere) (Pfeifer et al., 2007; Böhler et al., 2003; Lichti and Gordon, 2004). Studies on the influence of different types of materials and different colors show that the most suitable surfaces for scanning are light-colored surfaces with a diffuse reflection (Bucksch et al., 2007). In terms of color, black materials have high absorbability properties; therefore, they reflect a small amount of signal back to the laser source (Clark and Robson, 2004). Shiny materials such as metal or mirroring surfaces are difficult to measure due to the specular reflection of these materials. When a surface with reflective material is scanned, few or no signals are returned back to the laser scanner (Křemen et al., 2006).

To obtain a 3D point cloud, the scene is scanned from different positions around the considered object. The ideal set-up for scanning a surface of an object is to position the laser scanner in such a way that the laser

beam is near perpendicular to the surface. Due to scanning conditions, such an ideal set-up is in practice not possible. The different incidence angles of the laser beam on the surface result in 3D points of varying quality. Here we define the incidence angle as the angle between that surface normal that is pointing in the surface, and the incoming laser beam direction. In general it is assumed that the lower the incidence angle, the higher the accuracy of the range distance measurement. The focus of this paper is to study the quality of range measurements as a function of one component of the error budget: the scan angle. More specifically, the precision or noise level and relative intensities are compared for different angles of incidence. As it is known that the remission properties of the scanned surface have a large influence on these parameters as well, Bucksch et al. (2007), one more bright and one more matt plate is scanned. What is not investigated here are the accuracies of the scan points for different angles.

The influence of the incidence angle on the scan quality is studied using a horizontally rotating plate. By horizontal rotations of the plate, the scans cover all the horizontal incidence angles. The laser scanner LS880 HE80 from FARO (FARO, 2007) is used. The rotational device, on which the plate is fixed, enables horizontal rotations of the plate. As this device is not very accurate in practice, the real orientation of the plate with respect to the scanner at a certain orientation setting is reconstructed from the point cloud data. Given the orientation of the plate as a whole, the incidence angle  $i$  is reconstructed for each laser beam hit. Phase based scanners use different mechanisms to rotate horizontally and vertically. Therefore a decomposition of the incidence angle  $i$  in a horizontal and vertical component may reveal more detailed information on the scan angle error.

Incorporating the individual point accuracies in further processing steps such as scan registration, modeling or change detection is expected to result in end-products of better quality, and in end-products that are provided with an adequate quality description. Further research will focus on how to model error components and how to decompose a detected error in a certain scan point into error components. If the error budget of terrestrial laser scanning is well understood, it will be possible to design a measurement setup that fulfills certain quality requirements. At the end of this paper we give a first example.

This paper consists of four sections. The experiment set-up and data processing methodology is exposed in the next section. Then the results are discussed before arriving at the final section that contains conclusions and recommendations for further research.

## 2 Experiment setup and theoretically expected scattering results

In this section first the measurement set-up is explained, then it is shown how to obtain the incidence angle of a laser beam. In the remaining of the section some theory is presented on the scattering of light that will later be used to interpret the results of Section 3.

### 2.1 Measurement set-up

The laser scanner measurements quality is investigated using the experiment set-up as shown in Fig. 1, left. The laser scanner LS880 HE80 from FARO (FARO, 2007) is used. The laser beam of this laser scanner is deflected at  $90^\circ$  on a rotating mirror which determines the vertical field of view (rotations around  $X_s$  axis) of  $320^\circ$ . The head of the scanner rotates around the vertical axis  $Z_s$  to allow the horizontal field of view of  $360^\circ$ . A full resolution scan has typically around 28 million of points.

Two different plates are used for the experiment: a medium-density fibre board, the ‘wooden plate’ and a plywood board coated white, the ‘white plate’. A rotational device with a goniometer mounted on a tripod enables horizontal rotations of the plate, see Fig. 1. The plate’s orientation with respect to the rotational device is considered to be  $0^\circ$  when the terrestrial laser scanner in rest is parallel to the plate. The goniometer allows a rotation of  $2^\circ$  (estimated) precision. The results presented in this paper are obtained on three different range placements: 3.5 m, 5.5 m and 20.5 m.

All the scans are obtained in a near laboratory condition, under very similar environmental conditions. Therefore, the temperature or the humidity effects on the experiments are not taken into consideration. The

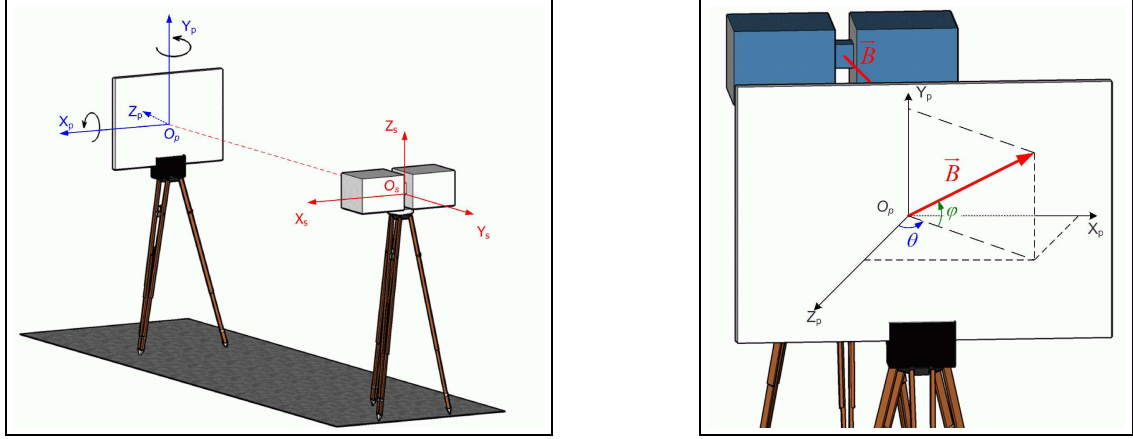


Figure 1: Experiment Set-up. Left: scanner- and plate-centered coordinate system. Right: the angle of incidence  $i$  (not shown) is defined as the angle between the laser beam vector  $\vec{B}$  and the normal to the plate  $Z_p$ . The incidence angle  $i$  can be decomposed into a horizontal angle  $\theta$  and a vertical angle  $\phi$ .

points that belong to the plate are selected manually from the resulting point cloud of each scan. The edges of the plate are not taken into consideration in this experiment. The manual selection results in 500 to 150000 points per scan, depending on the incidence angle and the range placement. The scans are exported as ASCII files (PTS format), which contain the points in a Cartesian coordinate system and a normalized intensity value. These data are analyzed in Matlab.

## 2.2 Determining the incidence angle

Each angle experiment results in a point cloud containing for each point a 3D position in a Cartesian coordinate system  $(X_s, Y_s, Z_s)$  with the laser scanner for center  $O_s$ . A least square plane is fitted to those laser points that represent the interior of the scanned plate. Then the points on the plate are transformed to an orthogonal coordinate system  $(X_p, Y_p, Z_p)$  centered at the center of gravity of the laser points representing the plate. Note that axes obtained with a principal component analysis (Gonzalez and Woods, 1992) vary depending on the shape of the selected scans. Therefore, a more robust method of constructing this coordinate system is opted. The normal vector  $\vec{N}_p$  pointing away from the scanner as obtained from a least square plane fit, forms the  $Z_p$ -axis of the plane. The projection of the  $Z_s$ -axis of the laser scanner on the plate will result in the  $Y_p$ -axis of the plate. The last component  $X_p$  is obtained by the cross product.

As the rotational device has a goniometer that gives a rotation of  $2^\circ$  (estimated) precision, the exact orientation of the plate is reconstructed before determining the incidence angle  $i$  of each individual laser beam. Each point of the scan is one hit of a laser beam on the surface. Let such a beam be represented by a vector  $\vec{B}$ , see Fig. 1, right. The angle between  $\vec{B}$  and the outward normal  $\vec{Z}_p$  of the plate is the incidence angle of the laser beam on the plate. In Fig. 1 the decomposition of the incidence angle  $i$  into a horizontal  $\theta$  and a vertical  $\phi$  angle component is shown. Studying the separate dependency of reliability parameters on the horizontal and the vertical component makes sense, because the scanner uses a different mechanism to produce vertical (via mirror) and horizontal (rotation of the whole device) angular increments. We focus here on the direct dependency of reliability parameters on the value of the un-decomposed incidence angle  $i$  however.

## 2.3 Scattering concept and expected intensity

In addition to the Cartesian coordinates, for each point in the point cloud an intensity value between 0 and 1 is given. This intensity value represents the amount of light received back to the scanner relative to amount of emitted light. The intensity is not a calibrated product. According to the manufacturers

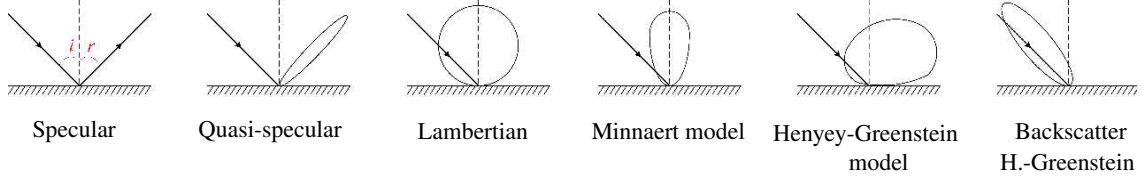


Figure 2: Schematic illustration of different surface scattering models (Rees, 1990).

of the laser scanner, the original intensity values are rescaled such that the final values correspond to the perceptual sensitivity of a human eye. In this way, an intensity ‘image’ of a scan is produced that resembles a well-balanced black and white photo of the scanned scene.

The strength of the signal received back at the scanner depends on the scattering behavior of the surface. Six main type of reflectivity are distinguished, (Rees, 1990), as illustrated in Fig. 2. Specular reflection occurs on a mirror-like smooth surface: light from a single incoming direction is reflected into a single outgoing direction. In contrast to the specular reflection, Lambertian reflectance appears when the surface scatters the light in all directions. In practice, scattering behavior is often described by mixed models as the Minnaert model or the Henyey-Greenstein model that result from combining the Lambertian with the specular model.

The spreading of light that hits a surface is described by the Bidirectional Reflectance Distribution Function, BRDF, that gives the ratio between the incoming and outgoing radiance. From the BRDF the simplified laser range equation, (Jelalian, 1992), is derived:

$$I = \frac{\pi \cdot P_E \cdot \rho \cdot \cos i}{4 \cdot R^2} \cdot \eta_{\text{atm}} \cdot \eta_{\text{sys}} \quad (1)$$

With  $I$  the intensity or received power at the scanner,  $P_E$  the emitted power, and  $\rho$  the reflectance of the material. The scanning geometry is incorporated by the incidence angle,  $i$ , and the surface range,  $R$ , from the laser scanner.  $\eta_{\text{atm}}$  and  $\eta_{\text{sys}}$  denote atmospheric losses resp. system losses

As every footprint is completely contained within the scattering area, i.e. the plate, the beamwidth is ignored in equation 1. The experiments are performed inside with short ranges, therefore the atmospheric losses are neglected. However, the system losses are not necessarily constant or linear. The system losses factor is here represented by a logarithmic function. By using two constants  $C_1$  and  $C_2$  that take ignored effects into account, Eq. 1 is simplified to represent the theoretical reflected intensity value as follows:

$$I = \frac{\rho \cdot \cos i}{R^2} \cdot \eta_{\text{sys}} \cdot C_1 + C_2 \quad (2)$$

### 3 Experimental results

In this section, the results from the experiments for determining the dependency on the scan angle of the intensity value and the noise level will be presented. Scanning the program as presented in Table 1 resulted in a total of 96 scans of the white and the wooden board. In the table,  $\theta$  indicates the horizontal orientation of a plate with respect to the scanner,  $\theta_-$  and  $\theta_+$  are the most extreme orientations and  $\Delta\theta$  indicates the applied angular increment.

#### 3.1 Intensity results

Fig. 3, left, represents the average of the received intensity values with respect to the reconstructed orientation of the white plate for each experiment. The standard deviations per average are plotted as well. The repeated experiments on the white board at 5.5 m distance, Fig. 3, left, red and blue curve, show that a

plate	distance	$[\theta_-, \theta_+]$	$\Delta\theta$	plate	distance	$[\theta_-, \theta_+]$	$\Delta\theta$
white	5.5 m	$[-90^\circ, 90^\circ]$	$5^\circ$	wood	3.5 m	$[-90^\circ, 90^\circ]$	$10^\circ$
white	5.5 m	$[0^\circ, 90^\circ]$	$10^\circ$	wood	5.5 m	$[0^\circ, 90^\circ]$	$2^\circ$
white	20.5 m	$[-90^\circ, 0^\circ]$	$10^\circ$	wood	20.5 m	$[-90^\circ, 0^\circ]$	$10^\circ$

Table 1: Performed experiments.

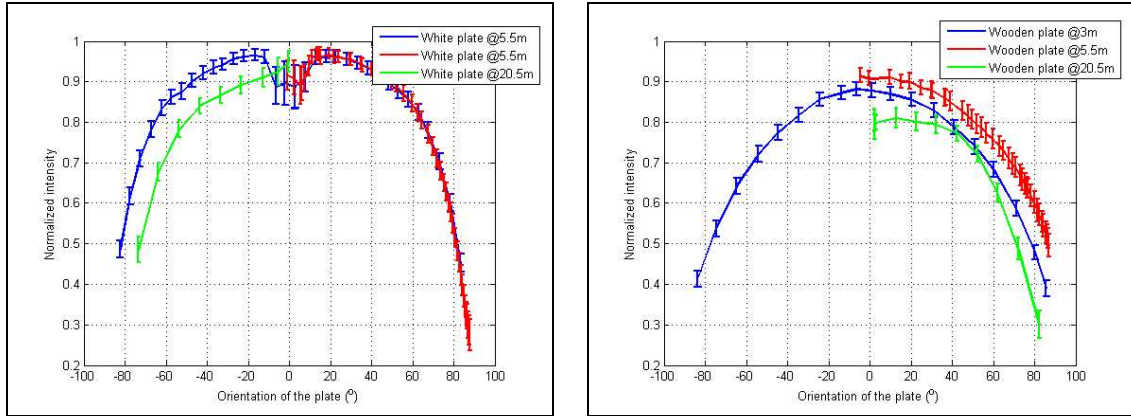


Figure 3: Average of the received intensity values and its standard deviation with respect to the orientation of the plate. Left: white plate, Right: wooden plate.

repetition of the experiment under the same controlled conditions but with a decreased angular step gives a consistent result.

The intensity measurement is symmetric around  $0^\circ$ . The results match our expectations. It is visible that at larger incident angles, the received intensity values are lower, due to the bigger footprint. Between scans, the plate was rotated clockwise for the 5.5 m experiment and counter-clockwise for the 20.5 m test. As expected, the rotation direction has no influence on smooth, planar surfaces. It is known that the average intensities decrease with increasing scan distance, but this effect is not directly measurable from our experiment setup, due to the automatic rescaling of the intensity values in the scanner software. Our results show that scanning at 20 m results in a similar pattern of decreasing intensity as scanning at 5.5 m.

It can be seen that for small incidence angles, the intensity slightly drops, while the st.dev. of the intensity increases. This effect is caused by saturation of the receiver unit of the scanner. Surface material that scatters with a specular component, like in e.g. the Henyey-Greenstein model, see Fig. 2, will show higher intensity values in case the angle of incidence coincides with the angle of reflection. For laser scanners this occurs only when the laser scanner hits the object surface perpendicular. When the receiving unit of the scanner receives more light than expected, an overshoot may occur. Note that this saturation effect is not occurring when the plate is at 20.5 m: in this case the returned intensity is lower anyway because of beam divergence and atmospheric losses.

The scattering behavior of the wooden plate with respect to the reconstructed orientation is shown in Fig. 3, right. The average intensity of the wooden plate is expected to be lower, because it reflects more diffuse and absorbs more energy. This may also explain that no clear saturation effect can be observed.

### 3.2 Noise level

Fig. 4 shows results of the planar adjustment for each scan in Table 1. For each scan the standard deviation of the residuals of a planar least square adjustment is plotted at the angle of orientation of the plane, with respect to the scanner. As expected the noise level increases for both plates with increasing incident angle and distance. In both cases the standard deviation is below 2 mm for the close by scans (3 m and 5.5 m) for

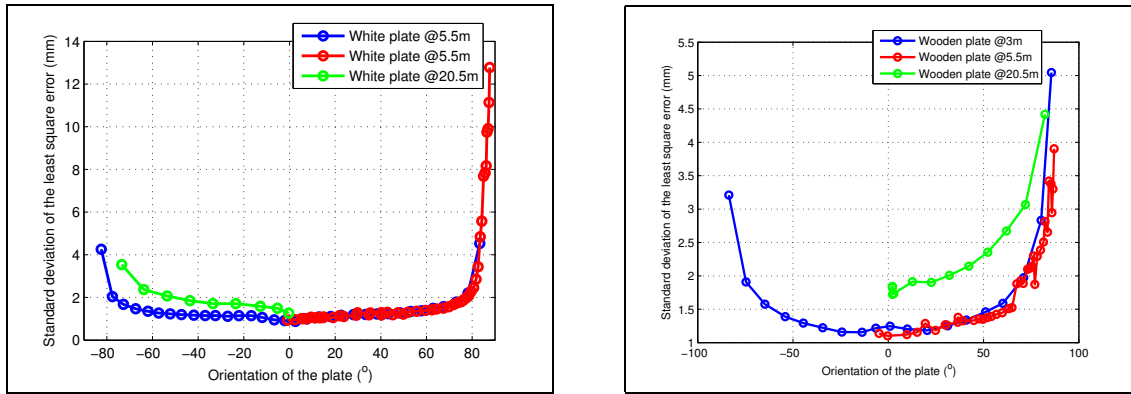


Figure 4: Standard deviation of the least square error plan fitting with respect to the orientation of the plate. Left: white plate. Right: wooden plate.

plate orientations of less than about 75 degrees. At close by distances, differences in behavior between the two plates are difficult to observe. The results of the 20.5 m scans show that the noise level of the wooden plate is maybe 30 % higher. This can maybe be explained by stronger light absorption of the wooden plate.

### 3.3 Experimental scattering models.

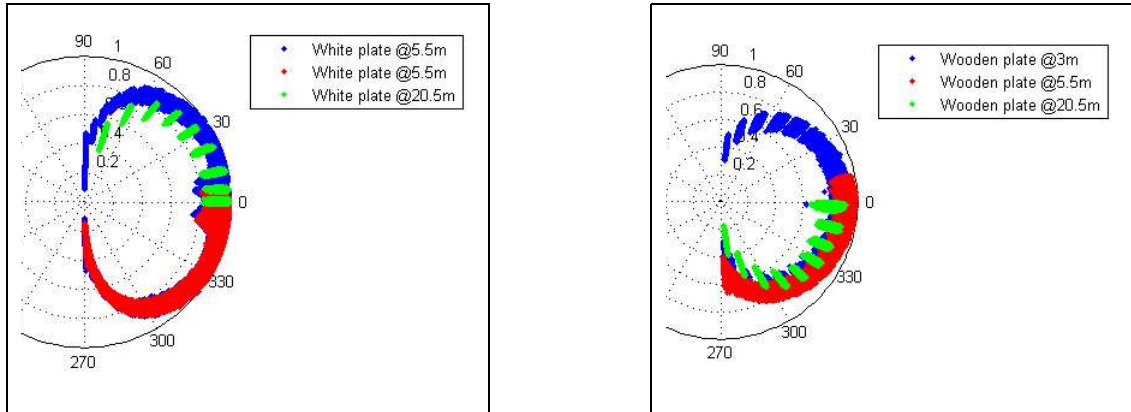


Figure 5: Received intensity values with respect to the horizontal incidence angle  $\theta$ . Left: white; Right: wooden.

In determining experimental scattering models, two different setups were considered. In the first setup the long side of the plate was placed (horizontally) in the rotational device. For the second setup, the experiment was repeated but now the short side of the plate was fixed in the device, that is, the plate was rotated over 90 degrees. In this way it could be considered if the material of the plate had different behavior when scanned from, say, left to right, than when compared to a scan from bottom to top. Such differences could be caused by e.g. an anisotropic grate pattern on the object surface.

Fig. 5 show the received intensity of each individual scan point with respect to the incidence angle of each point, for horizontally oriented plates. The result is represented in a polar coordinate system to visualize the scattering behavior of the material.

For each horizontal angle the standard deviation of the residuals of a least square adjustment are computed. Fig. 6 shows the resulting standard deviations in a polar representation for the white plate, left and the wooden plate, right. Even if the error increases with increasing incident angle, the standard deviation stays below 1 mm until  $\pm 60^\circ$ . Note that the stripes of errors observed at  $-60^\circ$  in Fig. 6, left are due to points

situated on the edge of the plate that are not correctly removed from the manual selection.

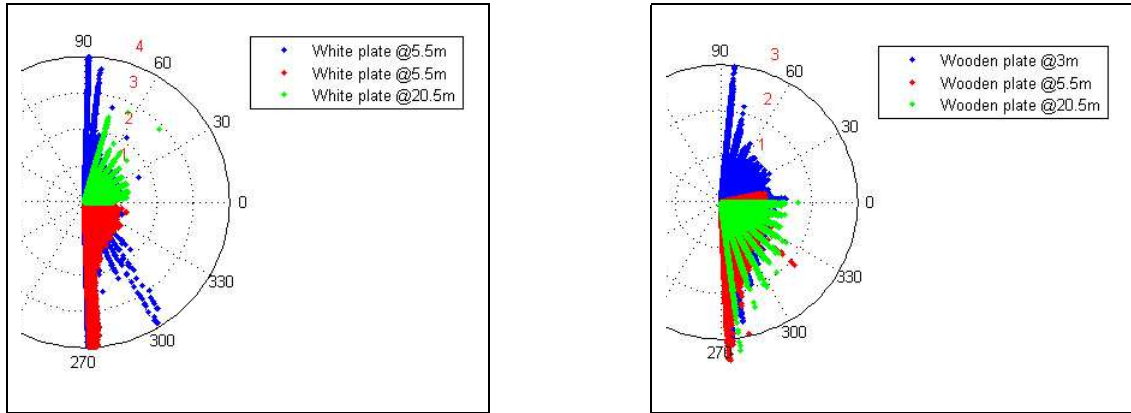


Figure 6: Scatterplot of the least square residuals of a planar fit with respect to the incidence angle  $\theta$ . Left: white; Right: wooden.

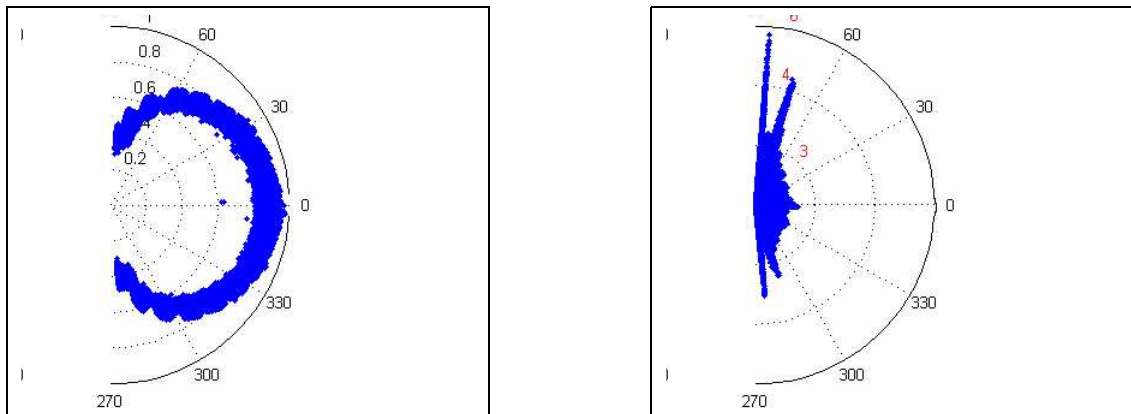


Figure 7: Received intensities (left) and least square error of planar fit (right) as a function of the vertical angle  $\theta$  for the wooden plate.

In Fig. 7, the intensity values, left, and residuals, right, for the vertically positioned wooden plate are shown. The rotational device containing the plate was placed at 3 m distance from the scanner. The scattering is similar to the previously obtained results for the horizontally placed plate. This behavior was expected, because the material has the same surface pattern in vertical and horizontal direction, as far as can be concluded from visual inspection. Fig. 7, right, shows that high noise levels occur for high vertical incidence angles. At incidence angles around 0 degree slightly higher residuals occur.

Even though the exact re-scaling procedure of the intensity values is unknown to the authors, some conclusions on the scattering behavior can be drawn. Both plates display mixed Lambertian-specular scattering characteristics. As expected, the white plate behaves more specular, with higher peak intensity, leading to saturation, near 0 degree incidence and a faster drop of intensity values for near parallel incidences. The authors were able to reproduce the laser range equation curves see Eq. 1, from the experimental results by choosing suited values for  $C_1$  and  $C_2$  and by using a logarithmic function for describing the system loss function  $\eta_{\text{sys}}$ .

## 4 Conclusions

The analysis of our experiments clearly state the following:

**High reflectance property** of the surface leads to re-scaled received intensity values at small incidence angles.

**The distance to the surface and the rotation direction** (clockwise vs. counterclockwise) does not influence the scattering behavior on smooth planar surfaces.

**Higher incidence angles and longer object distances** cause, as intuitively expected, higher noise levels. We experienced rapidly increasing noise for scan angles above 75 °. An increase in range seems to correspond to a vertical offset in the angle-noise level curve.

**Surface roughness** influences the range error measurement. The Rayleigh roughness criterion states that surfaces can be considered ‘rough’ if the RMS height of short-range surface variations exceeds one-eighth of the sensor weight length divided by the cosine of the incidence angle, (Rees, 1990). For laser light of 785 nm this means that the boundary between smooth and rough would occur at surface variations in the order of  $1 \times 10^{-7}$  m.

Future research should also consider the occurrence of possible angle dependent biases. In order to propagate the accuracy and precision of individual laser point in further processing steps like registration, modeling or change detection also changes in point density as caused by incidence angle changes should be taken into account, Lindenbergh et al. (2005). Ongoing research investigates the systematics behind the system function  $\eta_{sys}$  on the intensity value distribution. If real intensity values would be available, it would be easier to directly link received intensity values to the quality of individual scan points.

## References

- Böhler, W., Bordas Vicent, M., and Marbs, A. (2003). Investigating laser scanner accuracy. *IAPRS*, XXXIV(5/C15):696–701.
- Bucksch, A., Lindenbergh, R., and van Ree, J. (2007). Error budget of Terrestrial Laserscanning: Influence of the intensity remission on the scan quality. In *Proceedings GeoSiberia*, Novosibirsk, Russia.
- Clark, J. and Robson, S. (2004). Accuracy of Measurements made with a CYRAX 2500 Laser Scanner Against Surfaces of Known Colour. *IAPRS*, XXXV(B5):1031–1036.
- FARO (2007). *Laser Scanner LS 880 Techsheet*. Accessed September 2007, [http://www.faro.com/FaroIP/Files/File/Techsheets%20Download/04REF201\\_041\\_Laser\\_Scanner\\_LS.pdf](http://www.faro.com/FaroIP/Files/File/Techsheets%20Download/04REF201_041_Laser_Scanner_LS.pdf).
- Gonzalez, R. and Woods, R. (1992). *Digital image processing*. Addison Wesley Publishing Company.
- Jelalian (1992). *Laser Radar Systems*. Artech House.
- Křemen, T., Koska, B., and Pospíšil, J. (2006). Verification of Laser Scanning Systems Quality. In *Proceedings XXIII FIG Congress*, Munich, Germany.
- Lichti, D. and Gordon, S. (2004). Error propagation in directly georeferenced Terrestrial Laser Scanner point clouds for cultural heritage recording. In *Proceedings FIG WSA Modelling and Visualization*, Athens, Greece.
- Lindenbergh, R., Pfeifer, N. and Rabbani, T. (2005). Accuracy Analysis of the Leica HDS3000 and Feasibility of Tunnel Deformation Monitoring *IAPRS*, XXXVI(3/W3), Proceedings of Laserscanning 2005, Enschede, The Netherlands, 2005.
- Pfeifer, N., Dorninger, P., Haring, A., and Fan, H. (2007). Investigating terrestrial laser scanning intensity data: quality and functional relations. In *Proceedings International Conference on Optical 3-D Measurement Techniques VIII*, Zurich, Switzerland.
- Rees, W. (1990). *Physical principles of remote sensing*. Cambridge University Press.